Check for updates

APPLIED SCIENCES AND ENGINEERING

A lab-on-a-silicon-chip platform for all-electrical antibiotic susceptibility tests with a sample-to-results time within 20 minutes

Zheqiang Xu[1], Victoria C. Nolan[1], Yingtao Yu[1], Petra Muir[2], Sanna Koskiniemi[2]*, Zhen Zhang[1]*

Copyright © 2026 The Authors, some rights reserved; exclusive licensee American Association for the Advancement of Science. No claim to original U.S. Government Works. Distributed under a Creative Commons Attribution NonCommercial License 4.0 (CC BY-NC).

Rapid antibiotic susceptibility tests (ASTs) are essential for quick selection of effective drugs to treat infections at an early stage. However, the most widely used phenotypic ASTs in clinical practice often require 24 to 48 hours of pre-culture enrichment and 4 to 20 hours of testing. They are too slow to guide therapy, even with the most rapid protocol. Here, we report a lab-on-a-silicon chip (LOSC) system, which integrates arrays of silicon nanowire field-effect transistor (SiNWFET) sensors with high-throughput cell-collection microfluidics for rapid ASTs. The microfluidics concentrate bacteria into picoliter-scale chambers within minutes, eliminating the need for pre-cultivation. Embedded SiNWFETs sensitively track antibiotic-induced metabolic pH shifts, enabling AST by detecting rapid metabolic inhibition in susceptible bacteria. Using an unbuffered culturing medium, LOSC achieves sample-to-result times within 20 minutes for clinically isolated uropathogenic *Escherichia coli* strains. With its electrical readout and compact design, LOSC offers a low-cost, rapid, and portable AST solution for point-of-care diagnostics.

INTRODUCTION

Antibiotic/antimicrobial resistance (AMR) poses a critical threat to global health (*1*, *2*), demanding rapid and accurate diagnostic tools to guide effective antibiotic therapy (*3*, *4*). Phenotypic antibiotic susceptibility tests (ASTs) can determine appropriate antibiotic treatments for bacterial infections, thus ensuring the use of effective antibiotics and preventing the spread of AMR (*5*–*9*). However, the most widely used phenotypic tests in clinical practice, such as broth microdilution and Kirby-Bauer disk diffusion (*10*), are culture-based and time-consuming, requiring 24 to 48 hours of pre-cultivation before the tests can start. Even with the most recent rapid AST protocol (*11*), the traditional test still takes 8 to 20 hours, which is too long for patients to wait for therapy. Genotypic AST, detecting specific genetic sequences associated with antibiotic resistance (*12*, *13*), can provide a more rapid test (1–3 hours) (*14*, *15*), but cannot detect previously unidentified resistance mechanisms (false negative) (*16*). In addition, genotypic tests can also give false positives, since the presence of a resistance gene is not always associated with actual resistance (*17*).

Over the past decades, numerous innovative phenotypic ASTs have been developed (*7*), including motion detection (*18*, *19*), impedance-based growth monitoring (*20*), electrochemical sensing (*21*, *22*), Raman-assisted metabolic method (*23*–*25*), and microfluidic-based optical methods (*17*, *26*–*28*). Among these, a promising strategy for rapid AST involves monitoring bacterial metabolism under antibiotic treatment (*29*–*31*). Since antibiotics alter metabolic processes before causing cell morphological changes or cell death (*32*–*34*), metabolic profiling can potentially be faster than monitoring the cell morphology or cell numbers to determine antibiotic efficacy.

We previously demonstrated bacteria metabolism monitoring using silicon nanowire field-effect transistors (SiNWFETs) (*35*). The SiNWFET sensors electrically monitor cell metabolism-induced pH changes in the culture media, profiling detailed metabolic responses of bacteria to different antibiotics. It achieved a rapid testing time within 30 minutes. However, this method requires a large volume of samples with high cell density (~10^9 cells/ml) to enable rapid pH changes, which necessitates a pre-cultivation step for clinical samples and extends the sample-to-result time.

To address this limitation, we further integrated SiNWFET sensor arrays with high-throughput cell-collection microfluidics to realize a lab-on-a-silicon chip (LOSC) system for rapid ASTs without the need for pre-cultivation. *Escherichia coli* (*E. coli*) was chosen as a model pathogen in this study because it causes approximately 85% of urinary tract infections (UTIs) in primary care (*17*). With an estimated 450 million UTI cases globally each year (*36*) and a high frequency of resistance to first-line antibiotics (*37*, *38*), the need for rapid UTI ASTs is urgent. UTI samples are clinically relevant if they contain 10^3–10^5 cells/ml of *E. coli* (*17*, *39*). In our LOSC system, the microfluidics can collect and concentrate *E. coli* from dilute samples into picoliter-scale culture chambers within 10 minutes. The concentration of cells will accelerate pH changes in the culture chambers. In addition, by using an unbuffered medium, the LOSC system can determine the drug effect on clinically isolated *E. coli* within 10 minutes, yielding a total sample-to-result time of under 20 minutes. We further evaluated the LOSC platform across different bacteria, validating both its microfluidic capture of additional uropathogens and its AST performance on the Gram-positive/Gram-negative bacterium. These results demonstrated a rapid electrical AST platform with significantly reduced requirements on sample preparation, which holds great promise for low-cost point-of-care applications.

RESULTS

The LOSC design and realization

The LOSC integrates a silicon sensor chip containing arrays of SiNWFET sensors, with cell-collection microfluidics, as illustrated in Fig. 1, A and B. (More details on the LOSC fabrication can be found in the Materials and Methods and figs. S1 to S4.) In microfluidics, arrays of microscale culture chambers are integrated between a front channel and a back channel, with connections via sieve-like loading channels and exit channels, respectively (Fig. 1A). The loading

[1]Ångström Laboratory, Division of Solid-State Electronics, Department of Electrical Engineering, Uppsala University, SE-75121 Uppsala, Sweden. [2]Department of Cellular and Molecular Biology, Uppsala University, SE-75124 Uppsala, Sweden.
*Corresponding author. Email: sanna.koskiniemi@icm.uu.se (S.K.); zhen.zhang@angstrom.uu.se (Z.Z.)

Downloaded from https://www.science.org at Uppsala University on August 12, 2026

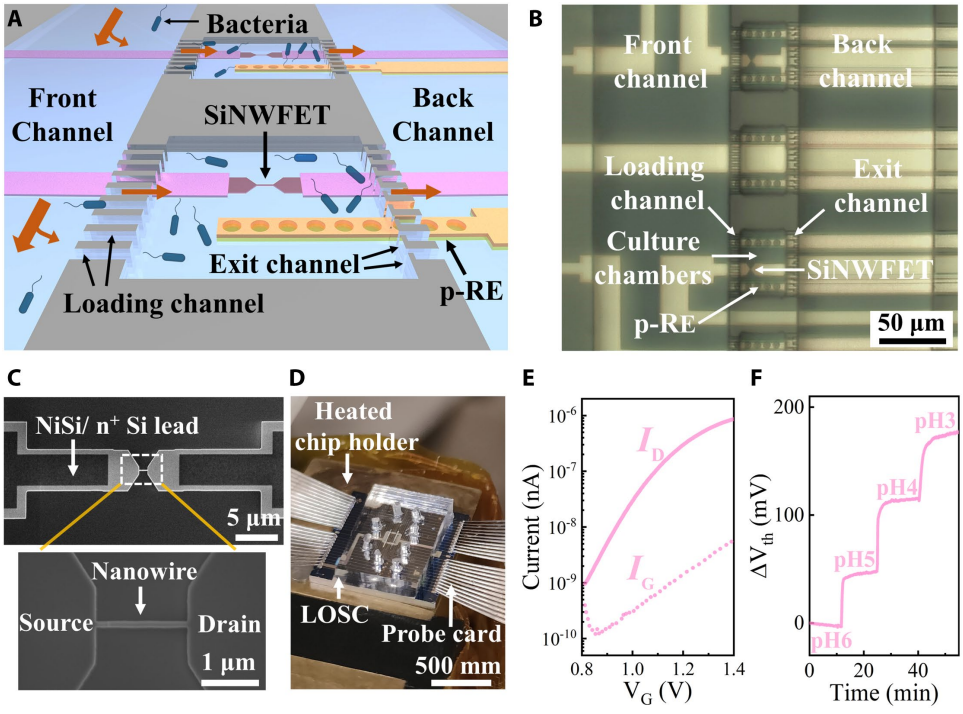

Fig. 1. The design of the LOSC. (**A**) Schematic illustration of the LOSC integrating a silicon sensor chip with cell-collection microfluidics. In microfluidics, microscale culture chambers are positioned between a front channel and a back channel, connected via loading and exit channels, respectively. Each culture chamber houses a SiNWFET sensor paired with an on-chip AgCl/Ag pseudo reference electrode (p-RE) on the silicon sensor chip. (**B**) Top-view optical image of the integrated LOSC. (**C**) Top-view scanning electron microscope (SEM) image of a SiNWFET. (**D**) Optical image of the measurement setup of the LOSC. (**E**) Transfer characteristics (I_D-V_G) of a SiNWFET measured at V_{DS} = 0.3 V in pH 7, 0.1 M NaCl at 37°C, with gate bias applied via the on-chip AgCl/Ag p-RE. (**F**) pH responses of the SiNWFET sensor in 0.1 M NaCl at 37°C. The shaded area along the solid lines depicts the standard deviations calculated from 3 SiNWFET sensors.

channels have a cross-sectional dimension of 2 μm in width and 1.5 μm in height, which permits the passage of *E. coli*. While the exit channels feature a minimum width of 0.5 μm to block *E. coli* escape with the liquid flow (Fig. 1B). Each culture chamber has a tiny volume of 35 pL (50 by 35 by 20 μm) and houses a SiNWFET sensor, together with the pairing AgCl/Ag pseudo reference electrode (p-RE) (*40*). The nanowire channel of the SiNWFET is 100 nm wide and 1.6 μm long (Fig. 1C).

To perform ASTs, the LOSC was connected to readout (HP 4155) via a probe card (Fig. 1D). We first characterized the SiNWFET sensor's pH response by applying gate voltage (V_G) through the on-chip AgCl/Ag p-RE. The transfer curve (I_D - V_G) in 0.1 M NaCl solution at pH 7 shows n-type behavior, a subthreshold swing of 120 mV/dec, I_{on}/I_{off} of 10^3, and gate leakage below 3 nA (Fig. 1E). For pH sensing, a constant V_G was applied, and I_D was recorded versus time. The shift of the threshold voltage of the SiNWFET (ΔV_{th}), induced by adsorption of protons to the pH sensing layer on the sensor surface (*35*), was extracted from the I_D change using the I_D-V_G curve (*40*). We observed a near-Nernstian ΔV_{th} response to pH with a sensitivity of 59.4 ± 0.8 mV/pH at 37°C (Fig. 1F). The noise of the SiNWFET sensor was evaluated from the power spectral density (PSD) of V_G (fig. S5). The root mean square (RMS) noise of V_G is below 1 mV, indicating that the device noise has a negligible influence on metabolic signal detection.

The workflow of the LOSC-based AST involves trapping bacterial cells into the culture chambers, introducing test media, and sealing both the front and back channels with oil to isolate the culture chambers (fig. S6 for details). This workflow ensures that ASTs are performed in a standardized medium independent of the original sample matrix, improving consistency and comparability. During bacterial trapping, for extremely dilute samples (<10^5 cells/ml), we employed a force-loading mode of the microfluidics to trap *E. coli*. In this mode, the outlet of the front channel is temporarily closed, directing the entire sample flow through the culture chambers before exiting via the back channel. This configuration enhances bacterial capture efficiency by ensuring that all fluid is forced through the chambers. For moderately dilute samples (>10^5 cells/ml), a bypass-loading mode was adopted to prevent clogging at the loading channel. In this mode, the outlet of the front channel remains open, allowing the majority of the sample to pass along the main channel, with a small fraction (~4.6% from simulations, fig. S8A) diverted into the chambers via side pathways.

Using an optical microscope, we observed uniform *E. coli* distribution across culture chambers after bypass-loading (Fig. 2A). One-way ANOVA analysis (see table S1) confirmed that there was no significant variation in cell distribution across chambers located at different positions, under either loading mode. Bypass-loading allowed capture of about 8 cells in each chamber in 8 minutes when using 5×10^6 cells/ml starting culture (Fig. 2B). Even using more diluted samples with 1×10^3 and 5×10^4 cells/ml, around 2–4 *E. coli* cells per chamber could be collected after 8 minutes of forced-loading (Fig. 2B).

The uniform cell distribution observed in Fig. 2A and table S1 is supported by numerical simulations. Under bypass-loading conditions,

Downloaded from https://www.science.org at Uppsala University on August 12, 2026

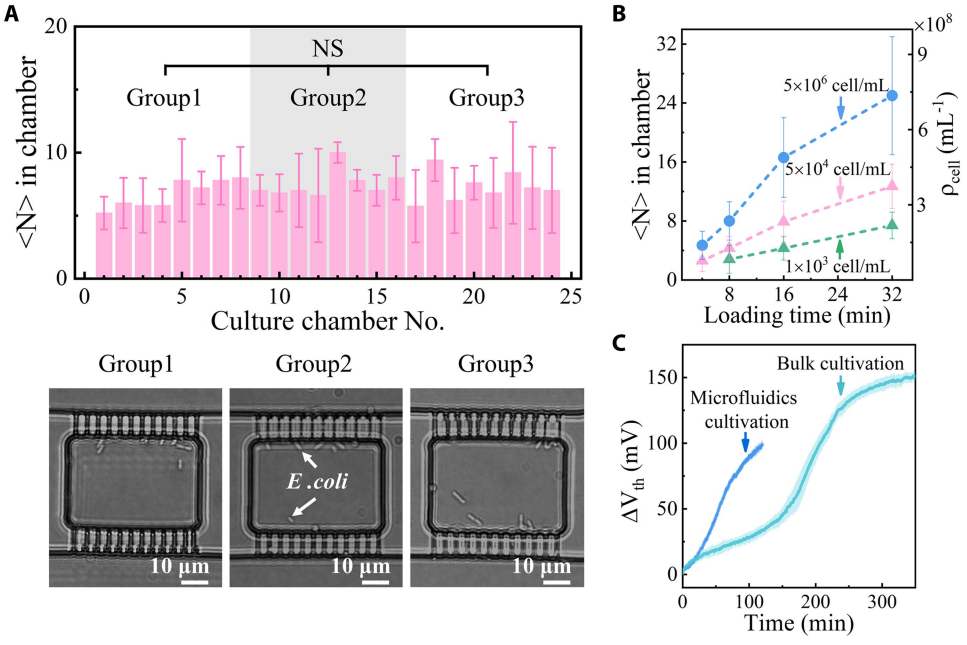

Fig. 2. *E. coli* capture in cell-collection microfluidics. (**A**) *E. coli* distribution across 24 culture chambers after 8-minute bypass-loading using a sample with 5×10^6 cells/ml at 8 μl/min. Bar plots show average cell numbers in chambers; error bars indicate standard deviations from four independent experiments. Chambers are sequentially numbered from inlet (No.1) to outlet (No.24) and grouped into three position-based groups. A one-way ANOVA test showed no significant (NS) differences between the groups ($p > 0.05$). Representative optical images from each group are shown below the bar plot. (**B**) Cell loading performance using samples with varying cell density. Force-loading mode was used for 1×10^3 (green) and 5×10^4 (pink) cells/ml; Bypass-loading was used for 5×10^6 (blue) cells/ml. Average number of cells per chamber ($< N >$-left axis) and corresponding effective volumetric cell density (ρ_{cell} - right axis) are plotted versus loading times (flow rate 8 μl/min). Effective volumetric cell density was calculated as $\rho_{cell} = < N > / V_{chamber}$. Error bars represent standard deviations across 24 chambers. (**C**) ΔV_{th} vs. time curve for *E. coli* cultivated in microfluidics chambers after 8-minute bypass-loading of 5×10^6 cells/ml sample and in a 100 μl PDMS container with 5×10^6 cells/ml sample (bulk cultivation, see fig. S11). LB media with 1 wt % glucose was used. The shaded areas represent standard deviations from three SiNWFET sensors.

the simulated flow fields (fig. S8B) indicate a self-regulated flow-partitioning effect: once bacteria are trapped at the exit channel, the local hydraulic resistance increases and redistributes the incoming flow toward less occupied chambers, promoting uniform loading. Under force-loading conditions, simulations show a nearly identical flow distribution among chambers (fig. S9, A and B), while the increased pressure drop across the loading channels (fig. S9D) efficiently forces bacteria into each chamber. Importantly, although force-loading operates at elevated pressure, the simulated pressure levels (fig. S9D) remain well below those that could damage the bacteria (*41*–*43*) or the microfluidic structures (*44*, *45*), whereas bypass-loading operates under much gentler pressure conditions (fig. S8D).

Beyond *E. coli*, the applicability of the cell-collection microfluidics to other UTI-related pathogens is demonstrated by the successful capture of *Klebsiella pneumoniae* and *S. aureus* in the microchambers (fig. S10).

Cell enrichment in a small chamber significantly accelerated the pH change induced by *E. coli* metabolism. The pH response of cultivating a 5×10^6 cells/ml sample was measured under two conditions: (i) bulk cultivation in a 100 μl PDMS container (detail setup is in fig. S11) (*35*) and (ii) microfluidics cultivation in the LOSC chambers after 8 minutes of bypass-loading, resulting in an average of 8 cells per chamber. Both experiments were conducted in Luria-Bertani (LB) medium supplemented with 1 wt % glucose at 37°C. The pH signal, reflected by ΔV_{th}, changes much more rapidly in the microfluidic cultivation than in bulk cultivation, as shown in Fig. 2C. This acceleration can be attributed to volumetric confinement: trapping on average ~8 cells in a 35 pL chamber corresponds to an effective volumetric density of approximately 3×10^8 cells/ml (Fig. 2B), which is nearly two orders of magnitude higher than the effective volumetric density used in the bulk cultivation (~5×10^6 cells/ml).

Reduction of test time with pH-unbuffered media

LB media contains numerous amino acids and peptides, which may have pH buffering capacity. A stepwise acid titration test (fig. S12) confirmed that LB retains a moderate pH buffering capacity, potentially slowing down the metabolism-induced pH changes. We therefore decided to investigate whether the response time could be shortened even further by replacing LB with an unbuffered medium. The experimental procedures followed those described in he "AST protocol" section. Culturing *E. coli* in the microfluidic chip (~8 cells per chamber) using physiological 0.9% NaCl with 1% glucose resulted in a 60 mV change in 20 minutes, as compared to 50 min in LB media (Fig. 3A). This demonstrates that reducing the buffering capacity of the culture media can accelerate pH change.

We next investigated how fast we could observe antibiotic susceptibility using the NaCl media. To assess the susceptibility of *E. coli* (MG1655) to Ampicillin (AMP), the ΔV_{th} vs. time response was monitored for the samples cultured in LB and NaCl media (add 1 wt % glucose) with and without AMP. In LB, both treated and untreated *E. coli* reached ΔV_{th} of 60 mV in 60 min, but whereas the untreated control sample continued to increase in ΔV_{th} to 120 min, the acidification halted in the AMP-treated sample after 70 minutes (Fig. 3B), suggesting that the antibiotic inhibited the metabolic activity of

Downloaded from https://www.science.org at Uppsala University on August 12, 2026

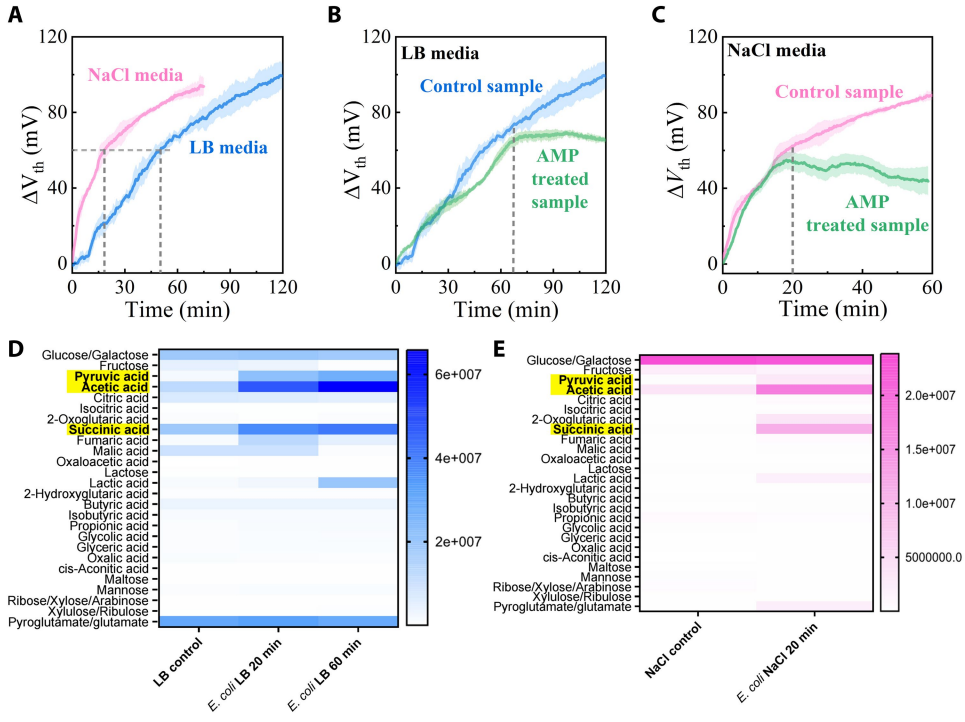

Fig. 3. ASTs for *E. coli* (MG1655) using the LOSC platform with different test media. (**A**) ΔV_{th} vs. time comparison for *E. coli* cultivation (~8 cells per chamber) in LB and NaCl media. (**B**) ΔV_{th} vs. time for *E. coli* in response to AMP (30 μg/ml) in LB media. (**C**) ΔV_{th} vs. time for *E. coli* in response to AMP (30 μg/ml) with NaCl media. The shaded areas represent the standard deviations calculated from three SiNWFET sensors. (**D**) Organic acid concentrations in LB media containing *E. coli* at 10^9 cells/ml after 20 and 60 minutes of cultivation. (**E**) Organic acid concentrations in NaCl media containing *E. coli* at 10^9 cells/ml after 20 minutes of cultivation.

E. coli. Viable counts confirmed decreased *E. coli* viability in LB with AMP (fig. S13A).

In NaCl, both cultures reached ΔV_{th} of around 60 mV in 20 min, after which the ΔV_{th} continued to increase for the untreated *E. coli*, whereas acidification was halted for the AMP-treated *E. coli* (Fig. 3C). Viable counts also confirmed decreased viability of the treated culture in NaCl (fig. S13B). The earlier halt in acidification observed in NaCl suggests that the use of unbuffered media can significantly accelerate AST.

To investigate whether the acidification of the media indeed arose from metabolic byproducts, we performed metabolomics analysis on the culture supernatant of *E. coli*. In both media, media acidification mainly originated from the secretion of acetate, pyruvate, and succinate (Fig. 3, D and E) as expected for *E. coli* during overflow metabolism (*46*). Further, OD measurements and microscopy (fig. S14) showed no apparent reduction in cell density over the two-hour culture, indicating that the pH changes arise from metabolism rather than cell lysis. Interestingly, less acids were produced in NaCl (Fig. 3E) as compared to LB at 20 min (Fig. 3D), even though a higher acidification was observed at 20 min (Fig. 3C). This further supports our findings that LB has a buffering capacity.

Rapid ASTs demonstration

Next, we used the LOSC to demonstrate rapid ASTs of lab strains of *E. coli* to three clinically used antibiotics against urinary tract infections (UTIs): AMP, Ciprofloxacin (CIP), and Nitrofurantoin (NIT) in NaCl. The AST procedures followed those described in he "AST protocol" section.

All three antibiotics reduced susceptible *E. coli* acid production, indicating suppressed metabolic activity. To define a quantitative susceptibility criterion, we used a ΔV_{th} difference threshold of 20 mV between treated and control samples, corresponding to the maximum standard error of ΔV_{th} for biological replicates in the LOSC AST measurements (fig. S16). The onset of susceptibility was defined as the earliest time point at which the ΔV_{th} difference exceeded this threshold (*17*, *28*). Using this criterion, susceptibility was detected at 30 min for AMP, 20 min for CIP, and 10 mins for NIT (Fig. 4, A to C). To validate the platform's ability to differentiate between antibiotic-susceptible strains and resistant strains, the same set of ASTs was performed using *E. coli* strains, resistant to AMP (SK4582), CIP (SK4686), and NIT (SK7394) strains (Fig. 4, D to F). The resistant strains did not reach the threshold difference of 20 mV in ΔV_{th} between antibiotic-treated and control samples over the test timeframe (Fig. 4, G to I), indicating that no metabolic arrest occurred in these resistant strains in response to the antibiotics. Validation through plating for viable cells confirmed that the antibiotics effectively killed susceptible *E. coli*, while the resistant strains remained viable during the treatments under the same time period (fig. S15).

To evaluate the alignment of our pH-based AST with standard MIC measurements, we performed dose–response experiments using three *E. coli* strains with CIP MICs of 0.012, 0.19, and 0.75 μg/ml determined by E-test (fig. S17). Our SiNWFET pH sensors were used to test these samples at a cell density of ~3×10^8 cells/ml. Increasing antibiotic concentration led to a reduction in metabolic activity (fig. S18, A to C), forming clear dose–response relationships. MIC-equivalent values were extracted using ΔV_{th} difference

Downloaded from https://www.science.org at Uppsala University on August 12, 2026

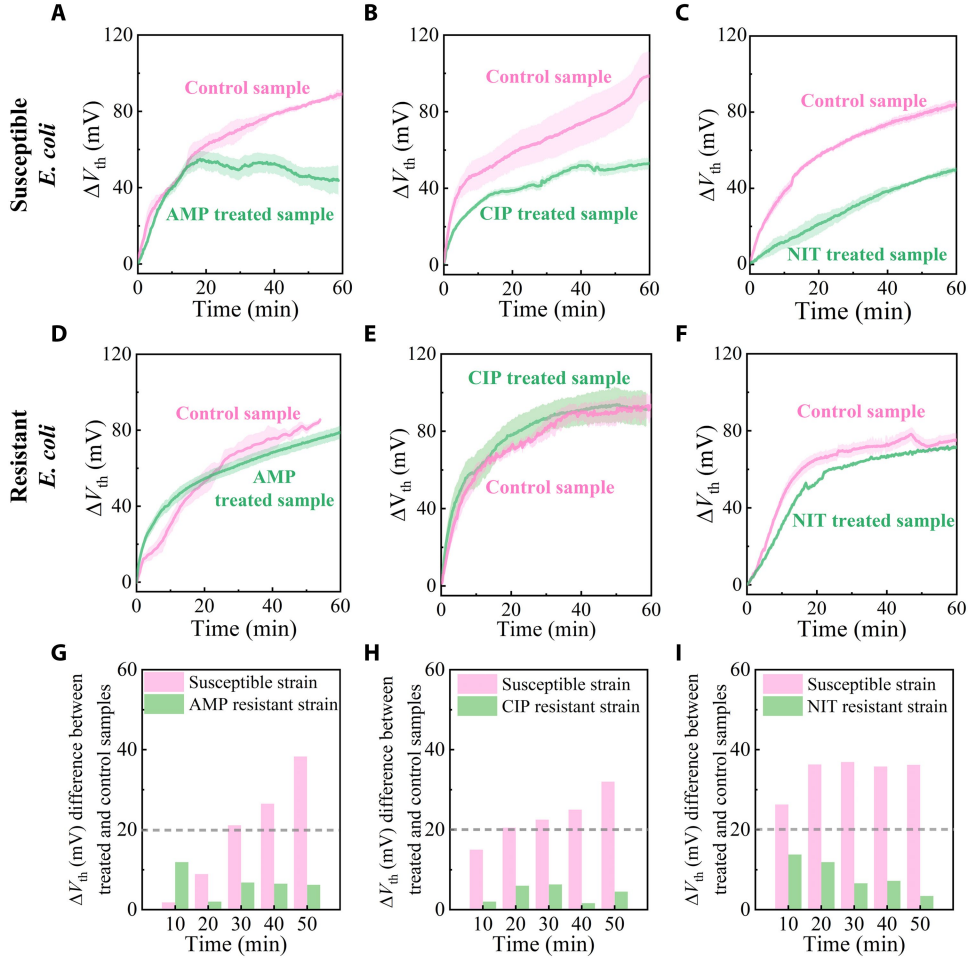

Fig. 4. ASTs of *E. coli* using the LOSC platform in 0.9 wt % NaCl (1 wt % glucose). ΔV_{th} vs. time for susceptible (**A** to **C**) and resistant (**D** to **F**) *E. coli* in response to [(A) and (D)] AMP (30 μg/ml), [(B) and (E)] CIP (2 μg/ml), and [(C) and (F)] NIT (200 μg/ml). The shaded areas represent the standard deviations calculated from three SiNWFET sensors. (**G** to **I**) ΔV_{th} difference between treated and control samples over time for the susceptible and resistant strains under the same antibiotic conditions [calculated from (A) to (F)]: (G) AMP (30 μg/ml), (H) CIP (2 μg/ml), and (I) NIT (200 μg/ml). The dashed lines indicate a 20 mV ΔV_{th} difference.

threshold-based criteria. As a general metric, susceptibility is defined when the ΔV_{th} difference exceeds 20 mV during the measurement period, yielding MIC-equivalent values of 2, 4, and 8 μg/ml (fig. S18D) and showing linear correlation with E-test MICs ($R^2 = 0.99$). Moreover, we can even limit the test duration to 5 minutes and define susceptibility as $\Delta V_{th} > 20$ mV within this period, to enable faster determination of MIC-equivalent values. This yields Fast-MIC-equivalent values of 8, 16, and 32 μg/ml (fig. S18E), which also show a strong linear correlation with E-test MICs ($R^2 = 0.99$). These consistent linear relationships obtained with both criteria demonstrate that the pH-based AST can be aligned with standard MIC measurements.

To evaluate whether the LOSC platform is applicable beyond *E. coli*, we performed AST measurement using *Staphylococcus aureus* (*S. aureus*), a Gram-positive bacterium. As shown in fig. S19A, the untreated *S. aureus* exhibited a rapid increase in ΔV_{th} followed by saturation (~100 mV) after 30 min, while NIT-treated cells showed a reduced acidification rate and a lower plateau (~70 mV), indicating antibiotic-induced metabolic inhibition. The kinetics and separation in the metabolic response of treated/control samples were consistent with those observed for *E. coli* (Fig. 4C). The susceptibility of *S. aureus* to NIT (fig. S19B) was further confirmed by the E-test, as shown in fig. S19B. These results demonstrate that our LOSC system can be used for both Gram-negative (*E. coli*) and Gram-positive (*S. aureus*) bacteria.

Rapid AST of clinical isolates

To assess the clinical applicability of the LOSC platform, we evaluated the antibiotic susceptibility of a clinical isolate of uropathogenic *E. coli* (UPEC 536) strain to two antibiotics: CIP (2 μg/ml) and NIT (200 μg/ml). The experimental procedures followed those described in the "AST protocol" section. The total sample-handling time was 10 mins (cell loading: 8 mins; culture media introduction: 1 min; and oil sealing: 1 min). Antibiotics reduced UPEC strain acid production as shown in Fig. 5, A and B, indicating suppressed metabolic activity. In both cases, a ΔV_{th} difference greater than 20 mV between treated and control samples was reached as early as 10 mins (Fig. 5, C and D). Notably, together with a 10-minute sample-handling time, the LOSC platform was able to resolve the susceptibility response with a sample-to-result time of within 20 minutes, demonstrating its potential for rapid phenotypic AST of clinical isolates.

Downloaded from https://www.science.org at Uppsala University on August 12, 2026

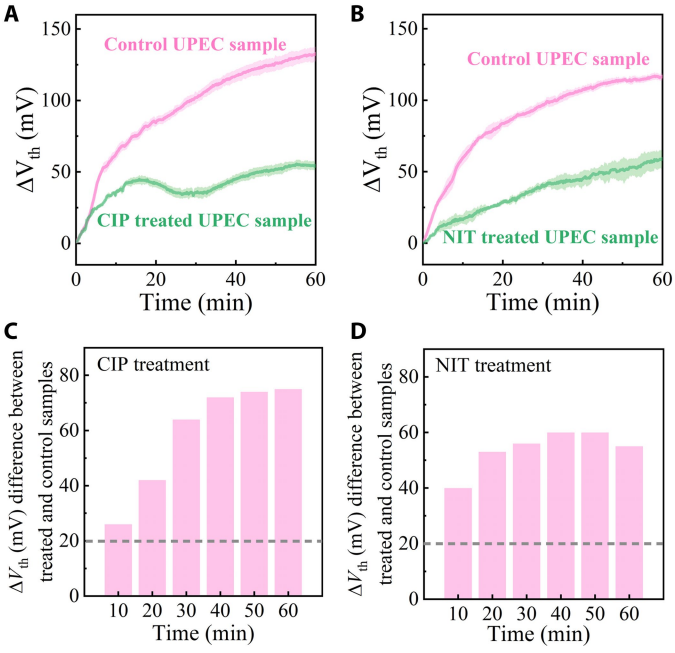

Fig. 5. ASTs for UPEC using the LOSC platform in 0.9 wt % NaCl (1 wt % glucose). ΔV_{th} vs. time for UPEC in response to (**A**) CIP (2 μg/ml) and (**B**) NIT (200 μg/ml). The shaded areas represent the standard deviations calculated from three SiNWFET sensors. ΔV_{th} difference between treated and control samples over time [calculated from (A) and (B)] in response to (**C**) CIP (2 μg/ml) and (**D**) NIT (200 μg/ml). The dashed lines indicate a 20 mV ΔV_{th} difference.

DISCUSSION

UTIs are the most frequent reason for antibiotic prescriptions. In standard clinical workflow (fig. S20), AST requires multiple steps of cultivation (*11*), making the total sample-to-result time somewhere between one to three days (*47*, *48*). This is too long to guide treatment choices. Instead, the prevalence of resistance is used to determine which antibiotic to currently use. A prevalence higher than 25% of resistant isolates can result in changed guidelines of treatment (*49*). This results in an overuse of last-resort antibiotics, when in most cases a cheaper, older antibiotic would be fully functional. Rapid ASTs could reduce the use of last-resort antibiotics, to a reduced cost for both the patient and society.

The long sample-to-result time mainly originates from the preculturing step required by conventional ASTs. Table 1 compares representative AST platforms in terms of working principle, sample compatibility, and testing time. Commercial clinical systems such as VITEK 2, Phoenix, and Sensititre are extensively validated and robust, but they require pure isolates and pre-cultivation, adding 24–48 hours to the total sample-to-result times. Many recently reported rapid AST approaches can shorten the testing time, but most still require a pre-culture step, which dominates the overall workflow and keeps the true sample-to-result time in the range of several hours to one or two days. A few AST platforms listed in Table 1 can perform direct-from-sample tests by integrating microfluidic (*17*, *28*, *39*) or magnetic-bead-based bacterial enrichment (*27*), and significantly shorten the sample-to-result time. Most of these systems rely on optical readouts based on bacterial growth, whereas our LOSC platform employs a purely electrical readout to profile cellular metabolism. Since our approach does not rely on observable morphological

Table 1. Comparison with representative AST platforms in terms of sensing principle, sample compatibility, testing time, and technology readiness level (TRL). Testing time refers to the duration of the AST test itself. Methods requiring pure culture samples typically involve 24–48 hours pre-cultivation of clinical samples. Technology readiness level (TRL) indicates technological maturity on a scale from 1 (early-stage concept) to 9 (fully validated and commercialized system) (*7*).

Principle	Sample compatibility	Testing time	TRL	Commercial name (Ref.)
Light absorbance measurement	Pure culture	5–18 hours	9	VITEK 2 (*62*)
Light absorbance measurement	Pure culture	4–16 hours	9	Phoenix (*63*)
Fluorescence detection	Pure culture	20–24 hours	9	Sensititre (*64*)
Bacterial nanomotion analysis	Short-term culture (6 hours)	2 hours	9	Resistell (*65*)
Bacterial mass detection	Positive culture	4.5 hours	9	LifeScale (*66*)
Single bacterial replication image	Urine specimen	1 hour	9	PA-100 AST (*67*)
Droplet shrinkage (subpopulations detection)	Pure culture	12 hours	4	(*57*)
Magnetic beads enrichment and microculture	Blood specimen	4–12 hours	6	(*27*)
Raman-assisted detection	Urine specimen	3 hours	6	(*23*)
SiNWFET-based pH monitoring	Pure culture	0.5 hour	4	(*35*)
This work (microfluidic enrichment and pH monitoring)	Urine specimen	10 min	4	

Downloaded from https://www.science.org at Uppsala University on August 12, 2026

changes, it has the potential to be faster than optical methods that monitor cell growth. It also provides a different phenotypic dimension and offers advantages in integrability and automation.

Against this background, the LOSC platform holds great promise for rapid AST directly on urine samples without the need for any preculture. To ensure efficient bacteria loading from urine, we also incorporated a filter region (*17*) at the inlet of the LOSC to prevent, e.g., white blood cells and debris from entering the microfluidic channels (fig. S3). Clinical UTIs are diagnosed from 10^3 to 10^5 cells/ml, depending on country (*50*, *51*). For UTI samples with $>10^4$ cells/ml, which is in the lower range for clinically relevant UTIs, sufficient bacteria loading (>3 cells per chamber) can be achieved within 10 minutes. Thus, our LOSC platform could, within 10 minutes, determine whether there is a clinically relevant infection at all. For severe bacterial infections, with more than 10^5 cells/ml, loading could be even faster. For samples containing fewer than 10^4 cells/ml, the bacterial loading step may become the time-limiting step in the LOSC workflow. To address this, loading efficiency could be further improved by increasing the flow rate or reducing the volume of the culture chambers. Or, the samples could be centrifuged to concentrate the sample prior to loading.

Moreover, the modular architecture of the LOSC platform permits spatial tiling of microfluidic sensor units, supporting future expansion toward high-throughput configurations. The electrical readout is naturally compatible with multiplexed architectures, supporting future scaling toward higher-throughput implementations.

While this study primarily focused on AST for *E. coli*, the applicability of the LOSC platform to a Gram-positive bacterium, *S. aureus*, was also demonstrated (fig. S19). The LOSC platform can be further extended to other microbial species. Specifically, for slow-growing bacteria such as *S. aureus* small colony variants (SCVs) (*52*) and *Mycobacterium tuberculosis* (*53*, *54*), our metabolism-based AST, which monitors acid production rather than growth rate, has the potential to deliver results significantly faster than growth-based rapid AST methods. And as metabolic profiles of different pathogens vary (*35*), the LOSC-generated data could in the future be used for infection diagnosis and AST results concurrently in the same run.

Another promising direction for future development is the design of microfluidics capable of isolating individual bacterial cells for single-cell AST. High-throughput single-cell AST would enable detailed characterization of heterogeneity in antibiotic susceptibility within bacterial populations (*55*–*57*) and offer insights into the link between metabolic state and resistance (*34*, *58*–*60*). Moreover, in polymicrobial infections, single-cell analysis could help resolve species-specific susceptibility profiles, ultimately guiding more precise and effective antimicrobial therapies.

In summary, the LOSC AST platform offers an electrical, low-cost solution capable of performing rapid AST directly on UTI samples, achieving a sample-to-result time of under 20 minutes. This makes it a promising candidate for point-of-care diagnostics and timely clinical decision-making.

MATERIALS AND METHODS

Silicon sensor chip realization

The SiNWFET sensors were fabricated as previously reported (*35*, *61*), using standard silicon process technology on SOI wafers with a 55 nm thick, p-type (1×10^{15} cm^{-3}) doped top Si layer. The process flow is illustrated in fig. S1. In brief, the wafer was heavily n-doped by arsenic (As) implantation while the channel region was protected by photoresist during the implantation. The silicon nanowires with source and drain pads were formed by electron beam lithography (EBL) and reactive ion etching (RIE). To reduce series resistance, NiSi was formed on the n^+-Si leads connecting the SiNWFETs to the probe pads at the edges of the chip. Subsequently, a 4-nm-thick HfO_2, deposited by atomic layer deposition (ALD), served as both gate dielectric and liquid passivation. Finally, forming gas annealing (5% H_2/95% N_2) at 400°C for 30 minutes passivated oxide/silicon interface traps.

For AgCl/Ag p-REs integration (*40*), a 150 nm Ag layer with a 10 nm Ti adhesion layer was deposited via evaporation and patterned by lift-off. Photoresist (UVN 2300–0.5) covered the electrodes, with contact holes opened by EBL to expose Ag near the SiNWFETs, as shown in Fig. 1A. The exposed Ag was further treated with a $FeCl_3$ solution (0.1 M) for 30 seconds to form an AgCl layer.

Cell-collection microfluidics fabrication

The cell-collection microfluidics were made from polydimethylsiloxane (PDMS) (Silgard 184; Dow Corning) using a silicon mold fabricated using lithography and RIE. Each PDMS chip contains two independent microfluidic testing units, and each unit comprises a culture-chamber array consisting of 27 chambers. Details of the fabrication process are shown in figs. S2 and S3.

Bonding of silicon sensor chip with cell-collection microfluidics

We devised an aligner to align a SiNWFET and its pairing AgCl/Ag p-REs within each microchamber in the cell-collection microfluidics, as shown in Fig. 1B. Before alignment, both the silicon sensor chip and the cell-collection microfluidics underwent O_2 plasma treatment for surface activation. The details of the alignment and bonding process are represented in fig. S4.

Bacterial strains

The susceptible *E. coli* strain used in this study was *E. coli* K12 MG1655. The UPEC strain used in this study was UPEC536. The genotypes of each strain are listed in the table S2.

AST protocol

During AST, *E. coli* samples at an initial concentration of 1×10^6 cells/ml were introduced into the LOSC device via a syringe pump operating at a flow rate of 8 μl/min for 8 minutes, using the bypass loading mode. Under these loading conditions, the microchambers were expected to reach an average volumetric cell density of approximately 3×10^8 cells/ml (see Fig. 2B). Following cell loading, test media, with or without antibiotics, were perfused into the LOSC at the same flow rate (8 μl/min) for 1 minute. Subsequently, FC-70 oil was introduced into both the front and back channels at a flow rate of 0.5 μl/min for 1 minute to effectively seal the chambers. Throughout the AST process, the LOSC is placed on a chip holder, which is maintained at a constant temperature of 37°C. The surface of LOSC is covered by FC-70 oil to further prevent liquid evaporation.

Electrical measurement

Electrical measurements were carried out using an HP4155A semiconductor parameter analyzer. HP4155A is connected to the LOSC via a probe card for drain current measurement. Multiple SiNWFETs were measured simultaneously via a Keysight 34970A switch unit.

Downloaded from https://www.science.org at Uppsala University on August 12, 2026

First, the transfer characteristics I_D-V_G were recorded. Subsequently, the drain current I_D was monitored in real time under a constant source-drain voltage V_{DS} of 0.3 V and a constant gate voltage V_G applied relative to the on-chip AgCl/Ag p-RE. V_{DS} was set to 0.3 V to ensure that the SiNWFET operates in the saturation regime, thereby reducing I_D sensitivity to V_{DS} fluctuations and improving readout stability. During measurement, V_G was set within the subthreshold region. The recorded I_D values were then converted to ΔV_{th} using the previously acquired transfer curve (*40*).

E. coli metabolic byproducts analysis

Screening of 3-nitrophenylhydrazine (3-NPH) derivatized metabolites by liquid chromatography coupled to mass spectrometry (LC-MS) was performed at the Swedish Metabolomics Center in Umeå, Sweden. Information about reagents, solvents, standards, reference and tuning standards, and stable isotopes internal standards can be found in the Supplementary Materials.

Supplementary Materials

This PDF file includes:

Supplementary Text
Figs. S1 to S20
Tables S1 and S2
References

REFERENCES

1. GBD 2021 Antimicrobial Resistance Collaborators, Global burden of bacterial antimicrobial resistance 1990-2021: A systematic analysis with forecasts to 2050. *Lancet* **404**, 1199–1226 (2024).
2. Antimicrobial Resistance Collaborators, Global burden of bacterial antimicrobial resistance in 2019: A systematic analysis. *Lancet* **399**, 629–655 (2022).
3. T. Jesudason, WHO publishes updated list of bacterial priority pathogens. *Lancet Microbe* **5**, 100940 (2024).
4. M. Jangra, D. Y. Travin, E. V. Aleksandrova, M. Kaur, L. Darwish, K. Koteva, D. Klepacki, W. Wang, M. Tiffany, A. Sokaribo, B. K. Coombes, N. Vázquez-Laslop, Y. S. Polikanov, A. S. Mankin, G. D. Wright, A broad-spectrum lasso peptide antibiotic targeting the bacterial ribosome. *Nature* **640**, 1022–1030 (2025).
5. C.-A. D. Burnham, J. Leeds, P. Nordmann, J. O'Grady, J. Patel, Diagnosing antimicrobial resistance. *Nat. Rev. Microbiol.* **15**, 697–703 (2017).
6. A. van Belkum, T. T. Bachmann, G. Lüdke, J. G. Lisby, G. Kahlmeter, A. Mohess, K. Becker, J. P. Hays, N. Woodford, K. Mitsakakis, J. Moran-Gilad, J. Vila, H. Peter, J. H. Rex, W. M. Dunne Jr., the JPIAMR AMR-RDT Working Group on Antimicrobial Resistance and Rapid Diagnostic Testing, Developmental roadmap for antimicrobial susceptibility testing systems. *Nat. Rev. Microbiol.* **17**, 51–62 (2019).
7. G. Reszetnik, K. Hammond, S. Mahshid, T. AbdElFatah, D. Nguyen, R. Corsini, C. Caya, J. Papenburg, M. P. Cheng, C. P. Yansouni, Next-generation rapid phenotypic antimicrobial susceptibility testing. *Nat. Commun.* **15**, 9719 (2024).
8. S. Bertagnolio, Z. Dobreva, C. M. Centner, I. D. Olaru, D. Donà, S. Burzo, B. D. Huttner, A. Chaillon, N. Gebreselassie, T. Wi, M. Hasso-Agopsowicz, B. Allegranzi, H. Sati, V. Ivanovska, K. U. Kothari, H. H. Balkhy, A. Cassini, R. L. Hamers, K. Van Weezenbeek, WHO Research Agenda for AMR in Human Health Collaborators, WHO global research priorities for antimicrobial resistance in human health. *Lancet Microbe* **5**, 100902 (2024).
9. M. Stracy, O. Snitser, I. Yelin, Y. Amer, M. Parizade, R. Katz, G. Rimler, T. Wolf, E. Herzel, G. Koren, J. Kuint, B. Foxman, G. Chodick, V. Shalev, R. Kishony, Minimizing treatment-induced emergence of antibiotic resistance in bacterial infections. *Science* **375**, 889–894 (2022).
10. E. Matuschek, D. F. J. Brown, G. Kahlmeter, Development of the EUCAST disk diffusion antimicrobial susceptibility testing method and its implementation in routine microbiology laboratories. *Clin. Microbiol. Infect.* **20**, O255–O266 (2014).
11. E. Jonasson, E. Matuschek, G. Kahlmeter, The EUCAST rapid disc diffusion method for antimicrobial susceptibility testing directly from positive blood culture bottles. *J. Antimicrob. Chemother.* **75**, 968–978 (2020).
12. T. Charalampous, G. L. Kay, H. Richardson, A. Aydin, R. Baldan, C. Jeanes, D. Rae, S. Grundy, D. J. Turner, J. Wain, R. M. Leggett, D. M. Livermore, J. O'Grady, Nanopore metagenomics enables rapid clinical diagnosis of bacterial lower respiratory infection. *Nat. Biotechnol.* **37**, 783–792 (2019).
13. Q. Ruan, W. Ruan, X. Lin, Y. Wang, F. Zou, L. Zhou, Z. Zhu, C. Yang, Digital-WGS: Automated, highly efficient whole-genome sequencing of single cells by digital microfluidics. *Sci. Adv.* **6**, eabd6454 (2020).
14. P. Bradley, N. C. Gordon, T. M. Walker, L. Dunn, S. Heys, B. Huang, S. Earle, L. J. Pankhurst, L. Anson, M. de Cesare, P. Piazza, A. A. Votintseva, T. Golubchik, D. J. Wilson, D. H. Wyllie, R. Diel, S. Niemann, S. Feuerriegel, T. A. Kohl, N. Ismail, S. V. Omar, E. G. Smith, D. Buck, G. McVean, A. S. Walker, T. E. A. Peto, D. W. Crook, Z. Iqbal, Rapid antibiotic-resistance predictions from genome sequence data for *Staphylococcus aureus* and *Mycobacterium tuberculosis*. *Nat. Commun.* **6**, 10063 (2015).
15. N. G. Schoepp, E. M. Khorosheva, T. S. Schlappi, M. S. Curtis, R. M. Humphries, J. A. Hindler, R. F. Ismagilov, Digital quantification of DNA replication and chromosome segregation enables determination of antimicrobial susceptibility after only 15 minutes of antibiotic exposure. *Angew. Chem. Int. Ed. Engl.* **55**, 9557–9561 (2016).
16. M. J. Ellington, O. Ekelund, F. M. Aarestrup, R. Canton, M. Doumith, C. Giske, H. Grundman, H. Hasman, M. T. G. Holden, K. L. Hopkins, J. Iredell, G. Kahlmeter, C. U. Koser, A. MacGowan, D. Mevius, M. Mulvey, T. Naas, T. Peto, J. M. Rolain, O. Samuelsen, N. Woodford, The role of whole genome sequencing in antimicrobial susceptibility testing of bacteria: Report from the EUCAST Subcommittee. *Clin. Microbiol. Infect.* **23**, 2–22 (2017).
17. O. Baltekin, A. Boucharin, E. Tano, D. I. Andersson, J. Elf, Antibiotic susceptibility testing in less than 30 min using direct single-cell imaging. *Proc. Natl. Acad. Sci. U.S.A.* **114**, 9170–9175 (2017).
18. S. Kasas, F. S. Ruggeri, C. Benadiba, C. Maillard, P. Stupar, H. Tournu, G. Dietler, G. Longo, Detecting nanoscale vibrations as signature of life. *Proc. Natl. Acad. Sci. U.S.A.* **112**, 378–381 (2015).
19. G. Longo, L. Alonso-Sarduy, L. M. Rio, A. Bizzini, A. Trampuz, J. Notz, G. Dietler, S. Kasas, Rapid detection of bacterial resistance to antibiotics using AFM cantilevers as nanomechanical sensors. *Nat. Nanotechnol.* **8**, 522–526 (2013).
20. N. Jo, B. Kim, S.-M. Lee, J. Oh, I. H. Park, K. Jin Lim, J.-S. Shin, K.-H. Yoo, Aptamer-functionalized capacitance sensors for real-time monitoring of bacterial growth and antibiotic susceptibility. *Biosens. Bioelectron.* **102**, 164–170 (2018).
21. J. D. Besant, E. H. Sargent, S. O. Kelley, Rapid electrochemical phenotypic profiling of antibiotic-resistant bacteria. *Lab Chip* **15**, 2799–2807 (2015).
22. J. Wang, P. Hui, X. Zhang, X. Cai, J. Lian, X. Liu, X. Lu, W. Chen, Rapid antimicrobial susceptibility testing based on a bio-inspired chemiluminescence sensor. *Anal. Chem.* **94**, 17240–17247 (2022).
23. X. Yi, Y. Song, X. Xu, D. Peng, J. Wang, X. Qie, K. Lin, M. Yu, M. Ge, Y. Wang, D. Zhang, Q. Yang, M. Wang, W. E. Huang, Development of a Fast Raman-Assisted Antibiotic Susceptibility Test (FRAST) for the antibiotic resistance analysis of clinical urine and blood samples. *Anal. Chem.* **93**, 5098–5106 (2021).
24. W. J. Thrift, S. Ronaghi, M. Samad, H. Wei, D. G. Nguyen, A. S. Cabuslay, C. E. Groome, P. J. Santiago, P. Baldi, A. I. Hochbaum, R. Ragan, Deep learning analysis of vibrational spectra of bacterial lysate for rapid antimicrobial susceptibility testing. *ACS Nano* **14**, 15336–15348 (2020).
25. D. Bauer, K. Wieland, L. Qiu, A. C. Neumann-Cip, G. Magistro, C. Stief, A. Wieser, C. Haisch, Heteroresistant bacteria detected by an extended Raman-based antibiotic susceptibility test. *Anal. Chem.* **92**, 8722–8731 (2020).
26. H. Li, P. Torab, K. E. Mach, C. Surrette, M. R. England, D. W. Craft, N. J. Thomas, J. C. Liao, C. Puleo, P. K. Wong, Adaptable microfluidic system for single-cell pathogen classification and antimicrobial susceptibility testing. *Proc. Natl. Acad. Sci. U.S.A.* **116**, 10270–10279 (2019).
27. T. H. Kim, J. Kang, H. Jang, H. Joo, G. Y. Lee, H. Kim, U. Cho, H. Bang, J. Jang, S. Han, D. Y. Kim, C. M. Lee, C. K. Kang, P. G. Choe, N. J. Kim, M.-D. Oh, T. S. Kim, I. Kim, W. B. Park, S. Kwon, Blood culture-free ultra-rapid antimicrobial susceptibility testing. *Nature* **632**, 893–902 (2024).
28. V. Kandavalli, P. Karempudi, J. Larsson, J. Elf, Rapid antibiotic susceptibility testing and species identification for mixed samples. *Nat. Commun.* **13**, 6215 (2022).
29. J. Chen, Z. Miao, C. Ma, B. Qi, L. Qiu, J. Tan, Y. Wei, J. Wang, Bispecific metabolic monitoring platform for bacterial identification and antibiotic susceptibility testing. *ACS Sens.* **10**, 1470–1482 (2025).
30. C. Ocaña, S. Brosel-Oliu, N. Abramova, A. Bratov, Low-cost multichannel system with disposable pH sensors for monitoring bacteria metabolism and the response to antibiotics. *Instrum. Sci. Technol.* **49**, 288–303 (2021).
31. Y. Tang, L. Zhen, J. Liu, J. Wu, Rapid antibiotic susceptibility testing in a microfluidic pH sensor. *Anal. Chem.* **85**, 2787–2794 (2013).
32. M. A. Kohanski, D. J. Dwyer, J. J. Collins, How antibiotics kill bacteria: From targets to networks. *Nat. Rev. Microbiol.* **8**, 423–435 (2010).
33. M. A. Lobritz, P. Belenky, C. B. M. Porter, A. Gutierrez, J. H. Yang, E. G. Schwarz, D. J. Dwyer, A. S. Khalil, J. J. Collins, Antibiotic efficacy is linked to bacterial cellular respiration. *Proc. Natl. Acad. Sci. U.S.A.* **112**, 8173–8180 (2015).
34. M. Ahmad, S. V. Aduru, R. P. Smith, Z. Zhao, A. J. Lopatkin, The role of bacterial metabolism in antimicrobial resistance. *Nat. Rev. Microbiol.* **23**, 439–454 (2025).

Downloaded from https://www.science.org at Uppsala University on August 12, 2026

35. X. Xu, S. Chen, Y. Yu, P. Virtanen, J. Wu, Q. Hu, S. Koskiniemi, Z. Zhang, All-electrical antibiotic susceptibility testing within 30 min using silicon nano transistors. *Sens. Actuators B* **357**, 131458 (2022).
36. Z. Zeng, J. Zhan, K. Zhang, H. Chen, S. Cheng, Global, regional, and national burden of urinary tract infections from 1990 to 2019: An analysis of the global burden of disease study 2019. *World J. Urol.* **40**, 755–763 (2022).
37. S. Von Vietinghoff, O. Shevchuk, U. Dobrindt, D. R. Engel, S. K. Jorch, C. Kurts, T. Miethke, F. Wagenlehner, The global burden of antimicrobial resistance - urinary tract infections. *Nephrol. Dial. Transplant.* **39**, 581–588 (2024).
38. C. Mares, R.-C. Petca, R.-I. Popescu, A. Petca, R. Multescu, C. A. Bulai, C. V. Ene, P. A. Geavlete, B. F. Geavlete, V. Jinga, Update on urinary tract infection antibiotic resistance-A retrospective study in females in conjunction with clinical data. *Life* **14**, 106 (2024).
39. J. Avesar, D. Rosenfeld, M. Truman-Rosentsvit, T. Ben-Arye, Y. Geffen, M. Bercovici, S. Levenberg, Rapid phenotypic antimicrobial susceptibility testing using nanoliter arrays. *Proc. Natl. Acad. Sci. U.S.A.* **114**, E5787–E5795 (2017).
40. Z. Xu, Y. Yu, P. Solomon, Z. Zhang, Integration of AC bias-stabilized SiNRFETs with microscale Ag/AgCl pseudo-reference electrodes for lab-on-chip biosensing application. *Sens. Actuators B Chem.* **441**, 138000 (2025).
41. E. Rendueles, M. K. Omer, O. Alvseike, C. Alonso-Calleja, R. Capita, M. Prieto, Microbiological food safety assessment of high hydrostatic pressure processing: A review. *LWT Food Sci. Technol.* **44**, 1251–1260 (2011).
42. C. E. O'Reilly, P. M. O'Connor, A. L. Kelly, T. P. Beresford, P. M. Murphy, Use of hydrostatic pressure for inactivation of microbial contaminants in cheese. *Appl. Environ. Microbiol.* **66**, 4890–4896 (2000).
43. F. Si, B. Li, W. Margolin, S. X. Sun, Bacterial growth and form under mechanical compression. *Sci. Rep.* **5**, 11367 (2015).
44. S. R. A. Kratz, B. Bachmann, S. Spitz, G. Holl, C. Eilenberger, H. Goeritz, P. Ertl, M. Rothbauer, A compression transmission device for the evaluation of bonding strength of biocompatible microfluidic and biochip materials and systems. *Sci. Rep.* **10**, 1400 (2020).
45. C. L. Gonzalez-Gallardo, A. Díaz Díaz, J. R. Casanova-Moreno, Improving plasma bonding of PDMS to gold-patterned glass for electrochemical microfluidic applications. *Microfluid. Nanofluidics* **25**, 20 (2021).
46. A. J. Wolfe, The acetate switch. *Microbiol. Mol. Biol. Rev.* **69**, 12–50 (2005).
47. A. Farrar, P. Turner, H. El Sayyed, C. Feehily, S. Chatzimichail, S. Ta, D. Crook, M. Andersson, S. Oakley, L. Barrett, C. Nellaker, N. Stoesser, A. Kapanidis, Ribosome phenotypes for rapid classification of antibiotic-susceptible and resistant strains of *Escherichia coli*. *Commun. Biol.* **8**, 319 (2025).
48. A. van Belkum, C.-A. D. Burnham, J. W. A. Rossen, F. Mallard, O. Rochas, W. M. Dunne Jr., Innovative and rapid antimicrobial susceptibility testing systems. *Nat. Rev. Microbiol.* **18**, 299–311 (2020).
49. T. Thomas, B. Daniel, G. Christian, H. Charlotta, H. Olof, O. Gisela, V. Malin, W. Andreas, (Swedish strategic programme against antibiotic resistance (Strama) (2022).
50. A. L. Flores-Mireles, J. N. Walker, M. Caparon, S. J. Hultgren, Urinary tract infections: Epidemiology, mechanisms of infection and treatment options. *Nat. Rev. Microbiol.* **13**, 269–284 (2015).
51. G. Schmiemann, E. Kniehl, K. Gebhardt, M. M. Matejczyk, E. Hummers-Pradier, The diagnosis of urinary tract infection: A systematic review. *Dtsch. Arztebl. Int.* **107**, 361–367 (2010).
52. B. C. Kahl, K. Becker, B. Löffler, Clinical significance and pathogenesis of staphylococcal small colony variants in persistent infections. *Clin. Microbiol. Rev.* **29**, 401–427 (2016).
53. T. Schon, J. Werngren, D. Machado, E. Borroni, M. Wijkander, G. Lina, J. Mouton, E. Matuschek, G. Kahlmeter, C. Giske, M. Santin, D. M. Cirillo, M. Viveiros, E. Cambau, Antimicrobial susceptibility testing of *Mycobacterium tuberculosis* complex isolates - the EUCAST broth microdilution reference method for MIC determination. *Clin. Microbiol. Infect.* **26**, 1488–1492 (2020).
54. V. C. Nolan, L. Rafols, J. Harrison, J. J. Soldevila-Barreda, M. Crosatti, N. J. Garton, M. Wegrzyn, D. L. Timms, C. C. Seaton, H. Sendron, M. Azmanova, N. P. E. Barry, A. Pitto-Barry, J. A. G. Cox, Indole-containing arene-ruthenium complexes with broad spectrum activity against antibiotic-resistant bacteria. *Curr. Res. Microb. Sci.* **3**, 100099 (2022).
55. H. Nicoloff, K. Hjort, B. R. Levin, D. I. Andersson, The high prevalence of antibiotic heteroresistance in pathogenic bacteria is mainly caused by gene amplification. *Nat. Microbiol.* **4**, 504–514 (2019).
56. S. M. Amato, C. H. Fazen, T. C. Henry, W. W. K. Mok, M. A. Orman, E. L. Sandvik, K. G. Volzing, M. P. Brynildsen, The role of metabolism in bacterial persistence. *Front. Microbiol.* **5**, 70 (2014).
57. S. N. Agnihotri, N. Fatsis-Kavalopoulos, J. Windhager, M. Tenje, D. I. Andersson, Droplet microfluidics-based detection of rare antibiotic-resistant subpopulations in *Escherichia coli* from bloodstream infections. *Sci. Adv.* **11**, eadv4558 (2025).
58. J. M. Stokes, A. J. Lopatkin, M. A. Lobritz, J. J. Collins, Bacterial metabolism and antibiotic efficacy. *Cell Metab.* **30**, 251–259 (2019).
59. B. Peng, Y. B. Su, H. Li, Y. Han, C. Guo, Y. M. Tian, X. X. Peng, Exogenous alanine and/or glucose plus kanamycin kills antibiotic-resistant bacteria. *Cell Metab.* **21**, 249–262 (2015).
60. P. Bhargava, J. J. Collins, Boosting bacterial metabolism to combat antibiotic resistance. *Cell Metab.* **21**, 154–155 (2015).
61. X. Chen, Q. Hu, S. Chen, N. L. Netzer, Z. Wang, S.-L. Zhang, Z. Zhang, Multiplexed analysis of molecular and elemental ions using nanowire transistor sensors. *Sens. Actuators B* **270**, 89–96 (2018).
62. "VITEK 2 510(k) Substantial Equivalence Determination Decision Memorandum Assay Only" (Food and Drug Administration). https://www.accessdata.fda.gov/cdrh_docs/reviews/K161227.pdf.
63. "BD Pheonix 510(k) Substantial Equivalence Determination Decision Summary Assay Only" (Food and Drug Administration). https://www.accessdata.fda.gov/cdrh_docs/reviews/K173252.pdf.
64. "Sensititre AST Plates 510(k) Substantial Equivalence Determination Decision Summary Assay Only" (Food and Drug Administration). https://www.accessdata.fda.gov/cdrh_docs/reviews/K232310.pdf.
65. "Resistell AG-Developing Leading Rapid AST Solution". https://resistell.com/.
66. "Affinity Biosensors. LifeScale: Innovation in Phenotypic Susceptibility Testing". https://affinitybio.com/.
67. "Sysmex. PA-100 AST system". https://www.sysmex-europe.com/products/products-detail/pa-100-ast-system/.
68. A. C. Chang, B. H. Liu, Identification of characteristic macromolecules of escherichia coli genotypes by atomic force microscope nanoscale mechanical mapping. *Nanoscale Res. Lett.* **13**, 35 (2018).
69. L. Zhang, Z. Shen, Y. Chen, C. Ma, M. Huang, Y. He, G. Wang, D. Huang, B. Su, B. Jiang, Y. Luo, W. Li, M. Lian, X. Xu, X. Cheng, Z. Wang, X-ray irradiation of pseudomonas aeruginosa induces biogenesis of outer-inner membrane vesicles with potential as a vaccine against acute pneumonia. *J. Extracell. Vesicles* **14**, e70151 (2025).
70. F. Lamret, J. Varin-Simon, F. Velard, C. Terryn, C. Mongaret, M. Colin, S. C. Gangloff, F. Reffuveille, *Staphylococcus aureus* strain-dependent biofilm formation in bone-like environment. *Front. Microbiol.* **12**, 714994 (2021).
71. A. Taglialegna, L. Matilla-Cuenca, P. Dorado-Morales, S. Navarro, S. Ventura, J. A. Garnett, I. Lasa, J. Valle, The biofilm-associated surface protein Esp of *Enterococcus faecalis* forms amyloid-like fibers. *NPJ Biofilms Microbiomes* **6**, 15 (2020).
72. O. Hodek, J. Henderson, L. Argemi-Muntadas, A. Khan, T. Moritz, Structural elucidation of 3-nitrophenylhydrazine derivatives of tricarboxylic acid cycle acids and optimization of their fragmentation to boost sensitivity in liquid chromatography-mass spectrometry. *J. Chromatogr. B Analyt. Technol. Biomed. Life Sci.* **1222**, 123719 (2023).
73. "Breakpoint tables for interpretation of MICs and zone diameters. Version 14.0" (The European Committee on Antimicrobial Susceptibility Testing, 2024). http://www.eucast.org.

Acknowledgments: The device fabrication was done in the Ångström Microstructure Laboratory (MSL) at Uppsala University, and the technical staff of MSL are acknowledged for their process support. Swedish Metabolomics Centre, Umeå, Sweden (www.swedishmetabolomicscentre.se) is acknowledged for the screening of 3-NPH derivatized metabolites by LC-MS. The authors acknowledge the use of ChatGPT-5.5 (developed by OpenAI) to assist with language editing and refinement during the preparation of this manuscript. **Funding:** This work was partially supported by Olle Engkvist Foundation 214–0322, the Swedish Research Council under Grant VR 2019–04690, 2023-02925_3, and 2024–05176, and the Wallenberg Academy Fellow program under Grant KAW 2020–0190.
Author contributions: Conceptualization: Z.X., S.K., and Z.Z. Methodology: Z.X., Y.Y, S.K., and Z.Z. Investigation: Z.X., Y.Y, V.C.N., and Z.Z. Data curation: Z.X. and V.C.N. Validation: Z.X. and Z.Z. Writing-original draft: Z.X. Writing-review & editing: Z.X, V.C.N., Y.Y., S.K., and Z.Z. Formal analysis: Z.X., S.K., and Z.Z. Visualization: Z.X. Software: Y.Y. Resources: Z.Z., P.M. and S.K. Funding acquisition: S.K. and Z.Z. Project administration: S.K. and Z.Z. Supervision: S.K. and Z.Z.
Competing interests: The authors declare that a patent application related to this work has been filed by Z.Z., who is also the inventor. The international filing date is 18 January, 2024, with a priority date of 23 January, 2023. The application was published as WO2024/156586 A1 on 2 August, 2024. The patent family currently comprises three pending applications in China, Europe, and the United States. The respective application numbers are CN 2024800090279, EP 24701573.8, and US 19/149,931. **Data, code, and materials availability:** All data and code needed to evaluate and reproduce the results in the paper are present in the paper and/or the Supplementary Materials. This study did not generate new materials.

Submitted 11 August 2025
Accepted 24 June 2026
Published 31 July 2026
10.1126/sciadv.aeb2880

Downloaded from https://www.science.org at Uppsala University on August 12, 2026

Science Advances

A lab-on-a-silicon-chip platform for all-electrical antibiotic susceptibility tests with a sample-to-results time within 20 minutes

Zheqiang Xu, Victoria C. Nolan, Yingtao Yu, Petra Muir, Sanna Koskiniemi, and Zhen Zhang

Sci. Adv. **12** (31), eaeb2880. DOI: 10.1126/sciadv.aeb2880

View the article online
https://www.science.org/doi/10.1126/sciadv.aeb2880
Permissions
https://www.science.org/help/reprints-and-permissions

Downloaded from https://www.science.org at Uppsala University on August 12, 2026

Use of this article is subject to the Terms of service

Science Advances (ISSN 2375-2548) is published by the American Association for the Advancement of Science. 1200 New York Avenue NW, Washington, DC 20005. The title *Science Advances* is a registered trademark of AAAS.

Copyright © 2026 The Authors, some rights reserved; exclusive licensee American Association for the Advancement of Science. No claim to original U.S. Government Works. Distributed under a Creative Commons Attribution NonCommercial License 4.0 (CC BY-NC).